Int J Adv Manuf Technol (2009) 42:1118–1130
DOI 10.1007/s00170-008-1672-5

ORIGINAL ARTICLE

Finite-element analysis on wafer-level CMP contact stress: reinvestigated issues and the effects of selected process parameters

K.-S. Chen · H.-M. Yeh · J.-L. Yan · Y.-T. Chen

Received: 17 March 2008 / Accepted: 14 July 2008 / Published online: 6 August 2008
© Springer-Verlag London Limited 2008

Abstract Contact stress uniformity is a key issue for the performance of wafer-level chemical–mechanical planarization (CMP) and has been extensively studied during the past two decades. However, contact-stress-related issues are not consistently presented in the literature. In addition, a number of topics remain to be addressed in wafer-level contact analysis. The objective of this article is in twofold. First, it aims to provide a more detailed discussion and stress analysis of the inconsistent issues, including the definition of CMP uniformity, the stress indicator, and the effect of carrier films. Second, contact stress analyses of several important but rarely touched problems are also investigated. Topics to be investigated include: the effects of material hyperelasticity, the effects of a grooved pad, the effects of wafer warpage due to residual stress, and finally the possible advantages of a multizone loading manner. For the first category, this work proposes a new definition of CMP uniformity based on the width of the relatively flat zone. In addition, the contact stress distribution in terms of both von Mises and normal stress are also investigated and their relationship is qualitatively established. Furthermore, the importance of the carrier films is reinvestigated, and the conclusion indicates that their importance is not as significant as previously reported. The hyperelasticity of pad material primarily affects the pad deformation. The presence of pad grooves results in a net increase of contact stress, but the global tendency is unchanged. A warped wafer significantly reduces the contact stress uniformity. By contrast, the multizone loading manner can effectively improve the uniformity of stress distribution. Finally, the stress analyses presented are integrated with a graphic user interface to form a CMP computer-aided design system for further applications. The issues addressed and the conclusions obtained are important for improvement of CMP performance.

Keywords CMP · Contact stress · Finite-element analysis

1 Introduction

The chemical–mechanical polishing (CMP) process is a key fabrication route in state-of-the-art integrated circuit fabrication processes [1]. The global uniformity of the material remove rate (MRR) is critical for short-wavelength optical lithography and copper fabrication processes as well as for device yield considerations. The schematic plot for a CMP process is shown in Fig. 1. It consists of a wafer carrier, a carrier film, and a pad attached on a rigid platen. When planarizing the wafer surface, it is placed on the platen with a uniform external applied load. A chemical slurry is sprayed continuously on the pad. Both the wafer and the pad rotate and their relative motion brings the wafer in contact with aggregates in the slurry, which generates multiple actions, including the mechanical shearing and chemical reaction, to remove the material. The detailed mechanism of the CMP process is quite complicated and not yet fully described due to the complexity of the interaction between the structural, chemical, fluid, and material domains. Significant efforts have been conducted to develop a coupled model by investigators such as Kim et al. [2]. However, most work still relies on traditional phenomenological observation.

K.-S. Chen (✉) · H.-M. Yeh · J.-L. Yan · Y.-T. Chen
Department of Mechanical Engineering,
National Cheng-Kung University,
Tainan, Taiwan 70101
e-mail: kschen@mail.ncku.edu.tw

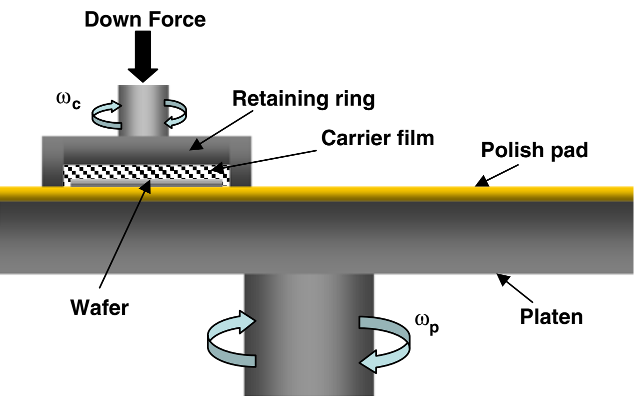

Fig. 1 The schematic plot for CMP process illustration

The MRR of the CMP process can be predicted by semiempirical formulas such as the Preston [3] equation, i.e.,

$$\mathrm{MRR}(\mu\mathrm{m/min}) = KPV, \quad (1)$$

where P is the interfacial pressure, V the relative velocity, and K a proportional constant, which is related to material prosperities, pad groove characteristics, slurry chemistry and aggregates, and even fluid dynamics [4]. Note that the Preston equation is merely one of the phenomenological expressions of the CMP process. Other expressions such as the model by Maury et al. [5], Zhang and Busnaina's [6] model, and the model proposed by Zhao and Shi [7] can also be used to describe the relationship among MRR, the sliding velocity, and the contact pressure.

According to Preston's equation, i.e., Eq. 1, the uniformity of a CMP process can be determined by the three major parameters shown in Eq. 1. For kinematics, it has been demonstrated that the operation shown in Fig. 1 could achieve uniform velocity distribution over the entire wafer [8]. On the other hand, the parameter K contains effects from virtually all the other aspects such as chemical reactions, fluid dynamics, and the geometrical and mechanical properties of the pads. It is thus usually too complicated to result in any useful mathematical modeling for the Preston constant. Consequently, most work on global CMP uniformity concentrates on discussing the contact stress distribution and the effects it imposes on the uniformity of the MRR over the entire wafer. This has been a benchmark problem of research in CMP stress analysis for many years. For example, Srinivasa-Murthy et al. [9] and Wang et al. [10] investigated the effects of various process parameters (such as material properties and the geometry of the carrier film and the polishing pad) on the wafer-scale MRR nonuniformity using finite-element analyses (FEA). They found that the MRR nonuniformity is highly correlated with the von Mises stress distribution and may be improved by changing pad compressibility. Lin et al. [11–15] have conducted a series of investigations on the relationship between the nonuniformity of the MRR and the material properties, as well as the geometry of the CMP pad and the carrier film via a self-developed FEA code. The conclusion was consistent with the observations of Srinivasa-Murthy. They further extended their analysis results to predict the MRR nonuniformity using fuzzy computation [13]. Fu and Chandra [16], on the other hand, using plate theory and the assumed-mode method, developing semianalytical formulas to predict the wafer normal contact stress (with the pad) under a uniform backside loading and the possible backside forcing pattern to achieve a uniform normal contact stress.

The above analyses were all based on flat wafers and pads. In fact, due to the existence of residual stress between the wafer and the film deposited on it, the wafer is not flat but slightly bowed. Discussion of the MRR or stress nonuniformity is lacking. Tseng et al. [17] related film stress to wafer curvature and developed a model based on shell theory to correlate the wafer curvature and the wafer scale nonuniformity in both contact stress and MRR.

1.1 Issues should be readdressed

Although research into wafer-level contact stress analysis has been ongoing for decades, many issues remain to be investigated. First, our literature review shows that there are inconsistencies in the extant literature on CMP contact stress modeling that require clarification. These issues are listed and briefly addressed below. Second, advances in CMP development impose the requirements on certain types of wafer-level contact stress analysis to obtain qualitative insight for the process optimization. The goal of this article, motivated by the above needs, is therefore to reexamine these inconsistent issues and perform more detailed and sophisticated FEAs to understand the effects of CMP process parameters.

The first category includes the definition of MRR uniformity in a typical wafer-level CMP analysis, the appropriate stress indicator, and the effect of carrier films. For the second category, issues to be discussed include the effects of the material constitutive law, the presence of pad grooves, the film residual stress effect, and novel multiple-zone loading schemes on the contact stress uniformity during CMP processes.

For the first category, many researchers have utilized von Mises stress as the stress indicator [9–15]. However, a number of studies have also applied the normal contact stress (with the corresponding polishing pad) as the stress indicator [16, 17]. Strictly speaking, these two stresses are not equivalent and their difference may be significant for certain situations. This issue is addressed in "Section 3.1." Furthermore, in Srinivasan et al. [9] and Lin et al. [11–15], the nonuniformity index was defined as the normalized difference between the stress levels at the center and at the

edge. However, as schematically shown in Fig. 2a, it is well known that a strong stress singularity exists at the wafer edge (i.e., by definition, such a nonuniformity index should be always infinity). In addition, the FEA results are also mesh dependent. However, in Lin and Lo, there are no special descriptions of how to refine the local mesh. Their nonuniformity index is thus questionable. Furthermore, the contact modeling between the wafer and the pad, generally treated as a critical issue in FEA, was not mentioned, while the effect of the wafer pad on the stress distribution appears unreasonable. A more sophisticated simulation should be reconducted to clarify the above issues. This issue is addressed in "Section 3.2." Finally, it is also important to point out that the benchmark problem for the wafer–pad contact is also not unique. For example, in some previous research, the benchmark problem included a rigid plate for applying uniform pressure, a carrier film, a wafer, and a polishing pad [11]. In these studies, the researchers argued that the role of the carrier film was very important and their material properties and dimensions directly affected the contact stress uniformity. However, in other studies, the benchmark problem was reduced to a uniform pressure applied on a wafer with a polishing pad underneath. This implies that the role of carrier films is merely to create a uniform loading and that its characteristics are not critical for MRR uniformity. As a result, it is worth reinvestigating the role of carrier film. In this work, this issue is evaluated and presented in "Section 3.3."

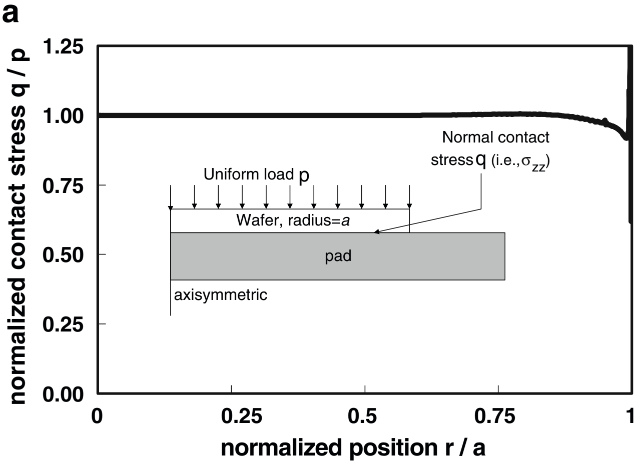

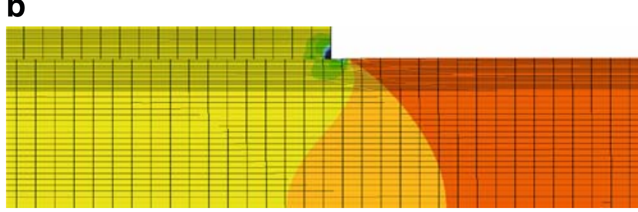

Fig. 2 A typical contact stress profile during CMP process. **a** Schematic contact stress distribution and **b** finite-element stress contour

1.2 New process parameters to be discussed

For the second category, the models proposed by Fu and Chandra [16] and Tseng et al. [17] were simplified semianalytical models. Many practical process parameters such as the hyperelastic nature of the pad materials and the finite thickness of pad cannot be considered in these models. A more detailed FEA is required to validate their model and to further quantify the significance of these practical parameters. This is addressed in "Section 4.1." Next, the surface of the pads contains grooves of different patterns for the purpose of slurry transportation. The influence of the grooves on the stress distributions is rarely discussed since this issue is highly case sensitive. In this work, a simplified model is used in conjunction with the generic finite-element model (FEM) mentioned above to yield a qualitative prediction of the stress distribution of a wafer on a grooved pad. This is reported in "Section 4.2." Furthermore, residual stresses existing in thin film usually induces warping of wafers. As a result, the contact stress distribution between a warped wafer and a flat pad is important for practical consideration. In "Section 4.3," the effect of wafer warpage is addressed and a map for governing the relationship between the contact stress uniformity with respect to initial wafer bow and the applied load is generated. Finally, the state-of-the-art CMP equipment allows several distinct backside pressure loadings at different zones to enhance the contact stress uniformity. To the best of our knowledge, there are only a few experimental reports on this specific topic [18] and the parameter setting relies purely on trial and error. As a result, it is worth performing a numerical analysis to provide a basis for process optimization that acts as a guideline for engineers. This issue is investigated in "Section 4.4."

The remainder of the paper presents the study. In "Section 2," the development of finite-element models for this work is presented in detail. The main analyses of the work, as indicated above, are then addressed in "Section 3" and "Section 4." "Section 5" summarizes the important observations and discusses the possible outcomes of this work. In "Section 6," the primary results of a CMP computer-aided design (CAD) which utilizes the stress analyses performed in "Section 3" and "Section 4" are demonstrated. Finally, the conclusion of this work is presented in "Section 7."

2 Construction of finite-element models

In order to perform the analyses mentioned in "Section 1," finite-element models should be constructed. The material properties and the structural geometries of the wafer (silicon) and pad (IC1010) shown in Table 1 are used as

Table 1 Baseline properties of the CMP pads, the wafers, and loading used for this work

Properties	Description
Dimension	Wafer radius, a_w 6 in. (about 150 mm) Pad radius, a_p 15.6 in. (about 390 mm) Wafer thickness, t_a 0.3 in. (about 0.762 mm) Pad thickness, t_p 1.2 in. (about 3 mm)
Loading	Uniform pressure 1~6 psi (about 6.6~40 KPa)
Material property	Wafer Young's modulus and Poisson's ratio, E_w 160 GPa, ν_w 0.3 Pad Young's modulus and Poisson's ratio, E_p 5 MPa, ν_p 0.1
Contact condition	Wafer and pad in contact at every point of the interface, small sliding
Boundary conditions	Axisymmetric; bottom of pad is restrained in vertical direction

the nominal parameters [19]. In total, there are five FEMs created for different applications, models A, B, C, D, and E. A summary of the FEMs is listed in Table 2. The generic model for model A is shown in Fig. 3. This axisymmetric finite-element model is constructed using the commercially available package ABAQUS [20] with 5,520 CAX8 axisymmetric elements and 16,080 nodes. The interface between the wafer and pad is modeled by a Hertzian contact [21] with small slidings. The thickness of the pad, however, is intentionally set to a very large value (300 mm) initially to approximate the physical model assumed in Fu and Chandra [16] for the purpose of verification at the very beginning. Figure 4 shows the comparison between our finite-element analysis and that predicted by Fu and Chandra. Both appear to agree with each other very well. This implies that the accuracy of the constructed finite-element model is verified.

Once the model is verified, more realistic features can be subsequently added to study the effects of various geometry, material, and processing parameters. First, a more realistic model (model B), containing the wafer and the polishing pad as well as the rigid carrier and the carrier film (Fig. 5), is used to evaluate the role of carrier films on the contact stress uniformity. Second, the initial bow of the wafer due to thin-film residual stress is a common and important feature of the semiconductor process and should be considered for CMP process. With the adding of axisymmetric shell elements (SAX2) to the backside of the wafer (to model the presence of the thin film) and the presence of initial stress, it is possible to create a desired controlled amount of wafer bow for the study, as shown in Fig. 6a (model C). Finally, the finite-element model for a flat wafer–grooved pad is also created, shown in Fig. 6b (model D) and the model used for evaluating multiple-zone loading is also presented (model E). All of these models are used to perform the study to evaluate the discrepancies and to investigate the effects of the selected process parameters on the contact stress uniformity. The results are presented in "Section 3" and "Section 4."

Table 2 Summary of the finite-element models

FEM model #	Description	Applications
A	Flat wafer vs. flat pad **2,2080 nodes, 5,520 CAX8 elements**	FEM verification Effect of material properties
B	Wafer carrier, carrier film, flat wafer, flat pad **43,600 nodes, 10,900 CAX8 elements**	Verification, effect of carrier film
C	Curved wafer vs. flat pad **22,080 nodes, 5,520 CAX8 elements** **280 nodes, 140 SAX2 elements**	Effect of wafer bow
D	Flat wafer vs. grooved pad Groove pitch= 5 mm, duty cycle=33 % **20,080 nodes, 5,020 CAX8 elements**	Effect of groove pad
E	Curved wafer vs. flatpad with two-zone loading Zone I: r=0-135 mm, Zone II: r=135-150 mm **22,080 nodes, 5,520 CAX8 elements**	Effect of multiple zone loading

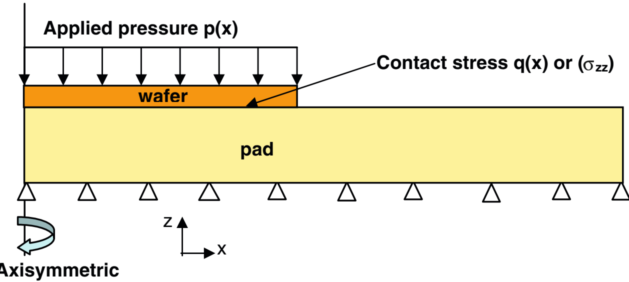

Fig. 3 The baseline finite-element model

3 Issues to be reinvestigated

3.1 Definition of uniformity

Traditionally, the performance index for measuring the wafer-level uniformity is the *Within Wafer Nonuniformity* (*WIWNU*). For a particular performance indicator *J*, *WIWNU* is defined as (*maximum J*−*nominal J*)/*nominal J* within a wafer. A typical normal contact stress of wafer in contact with a CMP pad is schematically shown in Fig. 2b. Using such a definition, the *WIWNU* for the MRR of the CMP process can be found by using the stress at the wafer center as the nominal stress and the stress at the edge as the maximum stress. However, it is well known that a singularity exists at the wafer edge. That is, the theoretical stress at the edge is actually infinity and the definition of the *WIWNU* for contact stress is thus questionable [11,12]. Here, we propose a new definition of the performance index for evaluating the contact stress uniformity. That is, instead of counting the percentage of stress variation as discussed above, it is also possible to evaluate the range of the relatively flat zone shown in Fig. 7 as the measure of the contact stress uniformity. However, since the curve at the "flat regime" is actually not completely flat but changes gradually, a stress variation range should be defined. For example, a 5% variation range could be used as the basis to find the range of the flat zone. The performance index is defined as the normalized flat zone length, which is defined as the radius of the flat zone, r^*, divided by the wafer radius, *a*, shown in Fig. 7. In this approach, in order to increase the CMP MRR uniformity, instead of seeking solutions to minimize the contact stress difference between the wafer center and the edge, the loading manner should be designed to enhance the range of the normalized flat zone.

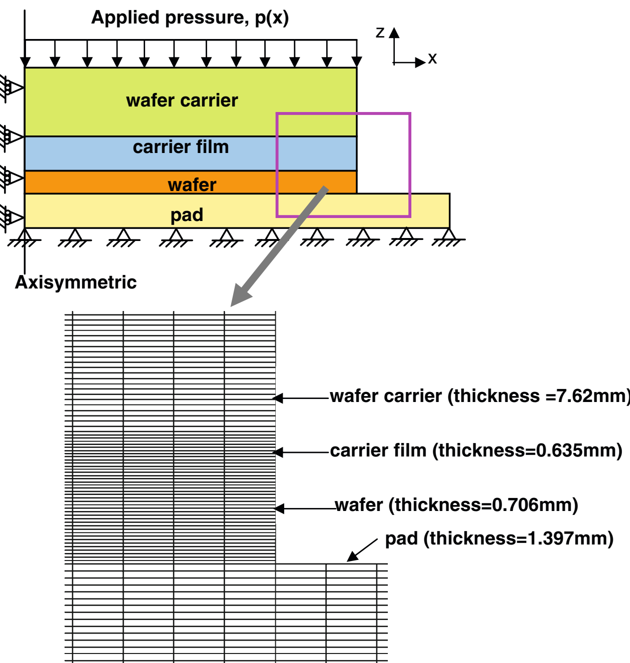

Fig. 5 A more detailed finite-element model containing wafer carrier and carrier film

3.2 Contact stress indicator: von Mises stress or normal contact stress

The original Preston's equation related the MRR of materials with the external applied pressure loading.

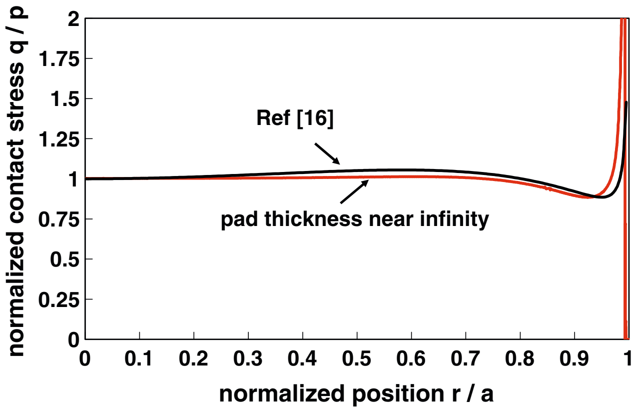

Fig. 4 The comparison between the contact stress distribution between the finite-element analysis and the analytical model [16]

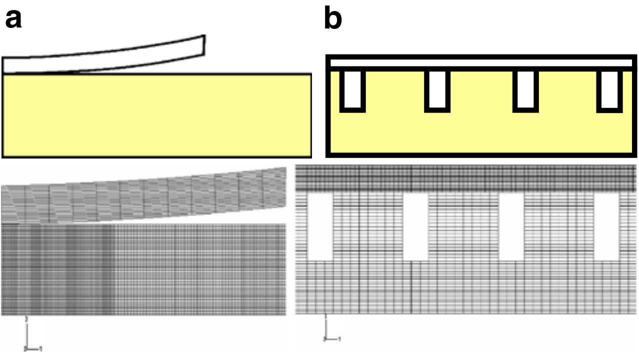

Fig. 6 Finite-element model for **a** wafer with initial warping contacts with flat pad (scale up by a factor of 1,000) and **b** flat wafer contacts with a grooved pad

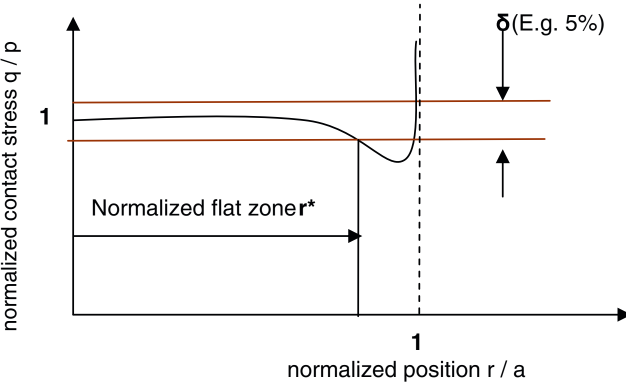

Fig. 7 The proposed performance index for representing the wafer-level contact stress uniformity

Runnels and Renteln [22] further modified Preston's equation by accounting for the deformation of the polishing pad. In their models, the expression is similar to that of the original Preston's equation except that the applied pressure loading is replaced by a shear stress. Since von Mises stress is actually an equivalent stress for yielding, which is strongly related to shear stress, it seems that these studies [9–15] used the appropriate stress index. On the other hand, Baker [23] presented a model based on the normal contact stress to explain the MRR nonuniformity. The pressure variation in the edge region is shown to match the nonuniform material removal. The predictions of this model agreed with the observed sizes of the edge effect over a range of polishing conditions. Based on this work, it seems that the choice of normal contact stress is also an appropriate stress index to describe the CMP process [16, 17]. In addition, microscopically, the material removal can be attributed to the friction force between the wafer and the aggregates. Since the friction force is proportional to the normal contact stress (times the associate friction coefficient), this also indicates that the normal contact stress is an appropriate stress index. However, the von Mises stress σ_{VM} is defined as [24]

$$\sigma_{\mathrm{VM}} = \frac{1}{\sqrt{2}}\left[\begin{array}{l}(\sigma_{rr}-\sigma_{zz})^2+(\sigma_{rr}-\sigma_{\theta\theta})^2+(\sigma_{\theta\theta}-\sigma_{zz})^2\\ +6\left(\sigma_{r\theta}^2+\sigma_{rz}^2+\sigma_{\theta z}^2\right)\end{array}\right]^{1/2}, \tag{2}$$

where σ_{rr}, $\sigma_{\theta\theta}$, σ_{zz}, $\sigma_{r\theta}$, $\sigma_{z\theta}$, and σ_{rz} are the six stress components in terms of a cylindrical coordinate. In general, the von Mises stress σ_{VM} is not equal to any particular stress component and the spatial distribution may also be different. Lin and Lo [11] investigated the magnitude of all stress components, concluding that the contribution of von Mises stress comes primarily from normal contact stress. This implies that the magnitudes of the von Mises stress and the normal contact stress are almost equal. However, their investigation was limited to the static condition and did not consider the effect of friction forces existing on the wafer surface during polishing. Further, they did not consider that such friction forces would actually increase the importance of the surface shear stress and that its magnitude is actually related to the friction coefficient. This surface shear stress is represented by σ_{rz} and $\sigma_{\theta z}$. From the relevant FEA, σ_{rr}, $\sigma_{r\theta}$, and $\sigma_{\theta\theta}$ can be neglected, making it possible to simplify Eq. 2 as

$$\sigma_{\mathrm{VM}} = \left(\sigma_{zz}^2+3\sigma_{rz}^2+3\sigma_{\theta z}^2\right)^{1/2}, \tag{3}$$

In addition, the kinetic friction force is the product of the relatively constant kinematic friction coefficient μ and the normal contact stress σ_{zz}. As a result, Eq. 3 can be further simplified to

$$\sigma_{\mathrm{VM}} = \sqrt{1+3\mu}\sigma_{zz}. \tag{4}$$

Figure 8 shows the von Mises stress distribution with different kinematic friction coefficients. For a small friction coefficient, the von Mises stress is essentially identical with σ_{zz}. For larger friction coefficients, the difference between von Mises stress and σ_{zz} becomes important. In a real-life scenario, if the CMP is operated in a hydrodynamic state, the friction coefficients are small and the normal contact stress and the von Mises stress would be essentially identical. On the other hand, if the CMP process involves dry contact, the friction coefficients could be high and these two stress quantities would have a considerable difference.

3.3 The role of carrier films

The main purpose of carrier films is to transmit a nonuniform loading to a uniform pressure on the front side of the wafer to be polished (see Fig. 5 or model B in Table 2). Some previous studies indicated that the geometry and material properties of carrier films significantly impact the contact stress uniformity. For example, Lin and Lo [11] indicated that the compliance of the carrier film signifi-

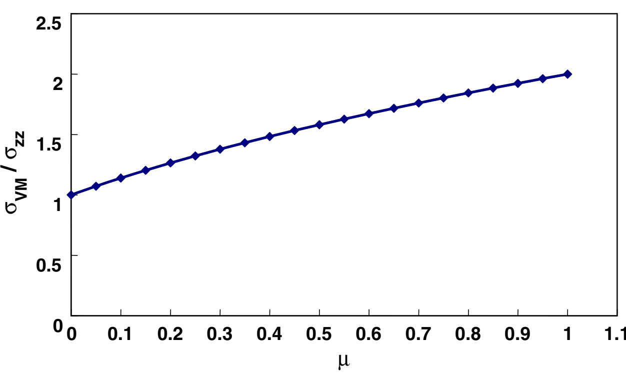

Fig. 8 The relationship between von Mises stress and contact stress with different kinematic friction coefficients

cantly affected the contact stress distribution. However, in other studies, the benchmark problem contains only a uniformly loaded wafer with a polishing pad (i.e., model A). This implies that it is not difficult to yield a uniform loading using a carrier film and that the thickness of the carrier film is not so critical. As a result, this issue should be carefully reinvestigated.

Figure 5 shows the finite-element model for the system containing a carrier film. The thickness of the carrier film is set as 0.635 mm. The corresponding contact stress distribution is shown in Fig. 5 for several different Young's moduli of the carrier film. The results show that the material properties of the carrier film have a slight impact on the contact stress distribution. However, the level of the effect is not as severe as that found by Lin and Lo [11]. We believe that this result is reasonable since the carrier, carrier film, wafer, and pad can be treated as a serially connected spring system and the reaction force is faithfully transmitted. That is, the total loading acted on the carrier film–wafer interface should approximately equal the load acted on the carrier regardless of the selection of carrier films (within a reasonable range). This argument is supported by the finite-element simulation results shown in Fig. 9. Another possible reason for the discrepancy is due to different definitions of *WIWNU*. For improper meshes, different carrier films may result in different edge stress (which is not correct) and, according to the definition of Lin and Lo, the stress nonuniformity would be enhanced. However, as addressed before, the results are mesh dependent. For these reasons, we believe that the importance of carrier films on the contact stress uniformity, as Lin and Lo argued, is exaggerated. The effect of the presence of both carrier and carrier film is minor, and the carrier film has been replaced by an air bag to faithfully transmit the applied load acted on the carrier onto the wafer surface for many state-of-the-art CMP equipments. Based on this study, the effect of carrier film is not important and the benchmark problem for evaluating CMP contact stress can be reasonably reduced to a uniformly loaded wafer contact with a polishing pad (i.e., model A).

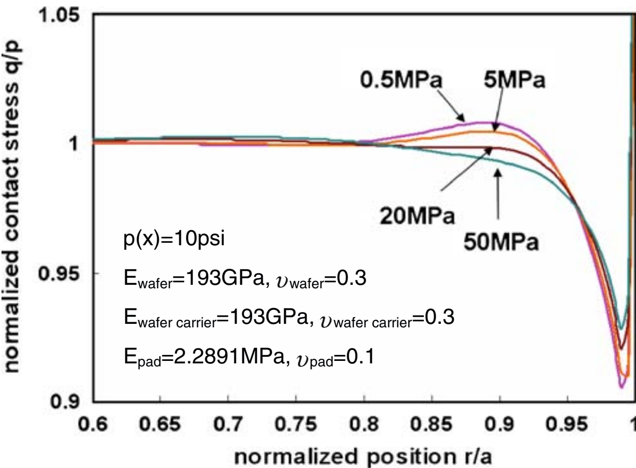

Fig. 9 The contact stress distribution with different Young's modulus of carrier films

4 Finite-element analysis: factors related to the wafer-level contact stress uniformity

4.1 Effect of hyperelasticity of polishing pads

The first issue to be investigated here is the influence of pad material properties between the flat wafer–flat pad contacts. Figure 10a shows the normal contact stress and the von Mises stress distribution along the radius for different Young's moduli. It is found that all the curves are similar, indicating that the normal contact stress is less dependent on the Young's modulus of the pad materials. This is reasonable because, for a semi-infinite media, the pad stress distribution can be obtained by a superposition process using the Cerruti solution as the Green's function in which

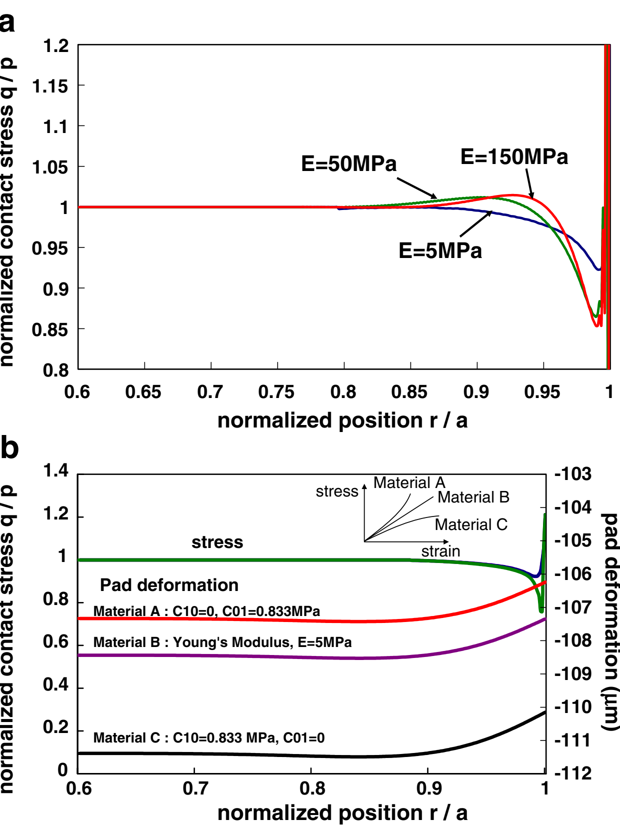

Fig. 10 Effect of pad material on the contact stress distribution for a flat wafer–flat pad contact **a** linear elastic pad with different Young's modulus and **b** hyperelastic pad with different Mooney-Rivlin coefficients

the stress distribution is independent of the material properties of the half space [25].

Next, the effect of material constitutive law is investigated. CMP pads are made of soft polymers, which in general can be treated as hyperelastic materials. In order to make the investigation more comprehensive, the linear elastic pad properties are replaced by a Mooney-Rivlin hyperelastic constitutive model [2, 20] and then the analysis is reperformed. The Mooney-Rivlin hyperelastic constitutive law for incompressible material can be expressed as [20]

$$W = c_{10}(I_1 - 3) + c_{01}(I_2 - 3), \tag{5}$$

where W is the strain energy and I_1 and I_2 are strain invariants, and c_{01} and c_{10} are two material constants. For incompressible media, the sum of c_{01} and c_{10} equals one sixth of the initial Young's modulus of an incompressible material. Figure 10b shows the comparison between the normal contact stress and the deformation distribution between linear elastic and hyperelastic materials. The linear elastic Young's modulus is assumed to be 5 MPa and the Mooney-Rivlin material parameters are adjusted so that the initial Young's modulus matches that of the linear elastic model. With two possible extremes indicated in Fig. 10b for a 200-KPa applied pressure, it shows that the stress distributions are similar except at the edge portion. However, the deformation of the pads shows considerable difference. The situations of $c_{10}=0$ (strain hardening, material C) and of $c_{01}=0$ (strain softening, material A) represent two boundaries for the deformation of a hyperelastic pad. As is clear, a few microns difference is observed in these cases and the difference in deformation field strongly affects the flow field and the built-in fluid pressure underneath the wafer, eventually changing the effective contact stress and, therefore, the MRR.

4.2 The effects of grooved polishing pads

The second issue to be investigated is the effect of the pad grooves. The corresponding finite-element model is shown in Fig. 6b. Note that the axisymmetric finite-element model assumes that the center of the wafer and the corresponding pad is the same. However, in reality, wafer location is eccentric with a distance and the effective pattern under the wafer changes constantly. This makes it difficult to reproduce the exact simulation scenario for a finite-element analysis. Nevertheless, useful qualitative information may be obtained from this idealized finite-element model, with useful results for future numerical studies and CAD development [8].

Figure 11 shows a typical normal contact stress distribution along the wafer radius direction. In comparison to a flat wafer subjected to the same pressure loading, the normal contact stress level is higher than the corresponding flat pad contact value at the contacted portion (and becomes zero at the uncontacted portion). The overall stress level is increased and the magnification ratio is approximately equal to the effective contact area ratio between these two cases. In addition, stress concentrations occur at the groove edges. Based on the observations, as shown in Fig. 11, the contact stress distribution for a wafer–grooved pad contact can be treated as an area ratio, A, times the original stress distribution $\sigma\times(r/a)$ and a switching function $s(r/a)$ ($s(r/a)$= 1 for ungrooved areas and $s(r/a)$=0 for grooved areas). This approximation may be very useful once the stress model is incorporated into a CAD model for providing instantaneous information for more realistic CMP situations.

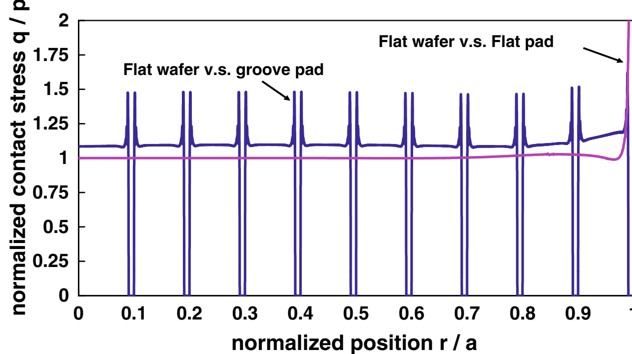

Fig. 11 The contact stress distribution for a flat wafer–grooved pad pair

4.3 The effect of residual stresses

CMP is usually used after copper electroplating or after dielectric deposition. The copper deposition process is usually accompanied by a considerable level of tensile residual stresses. On the other hand, the dielectric deposition may result in either tensile or compressive stresses. Such a stress tends to deform the wafer from its original flat shape to a bowed configuration. With the known material properties and geometric dimensions of the film and the corresponding substrate, the deformation can be converted into the film stress by appropriated mechanics. The well-known Stoney formula is usually used as the tool for this purpose. The relationship between the film stress, σ_{f}, and the radius of curvature, R, can be expressed as [26]

$$\sigma_{\mathrm{f}} = \frac{E_{\mathrm{s}} d_{\mathrm{s}}^3}{6(1-\nu_{\mathrm{s}}) R d_{\mathrm{f}}^2 \left(1 + d_{\mathrm{s}}/d_{\mathrm{f}}\right)}, \tag{6}$$

where E_{s} and ν_{s} are the Young's modulus and Poisson's ratio of the substrate, and d_{s} and d_{f} are the thickness of the substrate and the film, respectively. As a result, the traditional flat wafer and flat pad contact analysis may not adequately reflect the needs of practical CMP processes. A contact problem involving a bowed wafer versus a flat pad should be addressed.

One major problem for the contact stress is that the contact stress is no longer linearly proportional to the applied loading but rather a complicated relationship of the wafer bow and the applied loading. Figure 12 shows a typical finite-element stress contour for an applied loading of 1 psi and an initial wafer bow of ±150 μm caused by residual tensile or compressive stresses. It can be seen that both tensile and compressive stresses tends to deteriorate the uniformity. However, it is also worth pointing out that the convex shape (caused by tensile residual stresses) has a better CMP uniformity than the concave shape (caused by compressive residual stresses) under the same stress level.

Figure 13 shows a more comprehensive study of the relationship between the normal contact stress, the initial wafer bow (concave shape), and the applied pressure. The map indicates that, for situations with a low initial bow or a high applied load, the normal contact stress distributions are similar to those of the flat wafer–pad situation shown in “Section 4.1.” On the other hand, for a high initial wafer bow or a low applied loading, the normal contact stress distribution is less uniform, and even the contact between the wafer and the pad is lost. Figure 14 shows two typical normal contact stress distributions to illustrate the above arguments. For example, in Fig. 14a, with a relatively small initial bow and a relatively larger loading, both the tensile- and compressive-stress-induced wafer bows show less effect on the contact stress uniformity. On the other hand, in Fig. 14b, the contact stress uniformity is significantly degraded due to larger wafer bows and smaller loading. Again, as pointed out previously, the contact stress uniformity of wafer with tensile residual stress is slightly better than those of wafers with the same amount of compressive stress.

4.4 Multiple-zone applied loading

Finally, the effect of multiple loading zones is studied. Fu and Chandra [16] developed a semianalytical approach to calculate the necessary external loading distribution resulting in a uniform normal contact stress. Theoretically, such a nonuniform external loading can be approximated by a series of discrete uniform loadings. In modern CMP equipment, instead of using a single uniform load, it is allowed to replace this single valued load by several

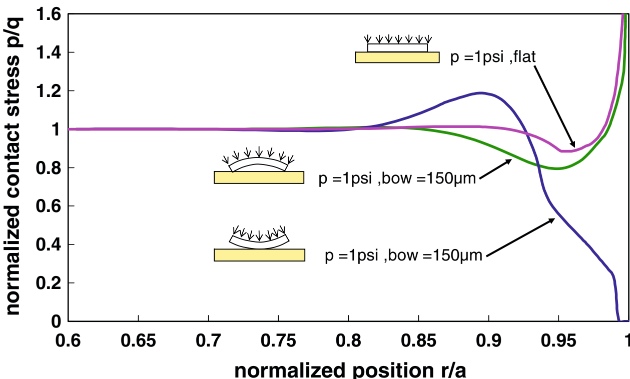

Fig. 12 The contact stress distribution between a flat pad and warping wafers with an initial bow of ±150 μm subjected to 1 psi uniform load

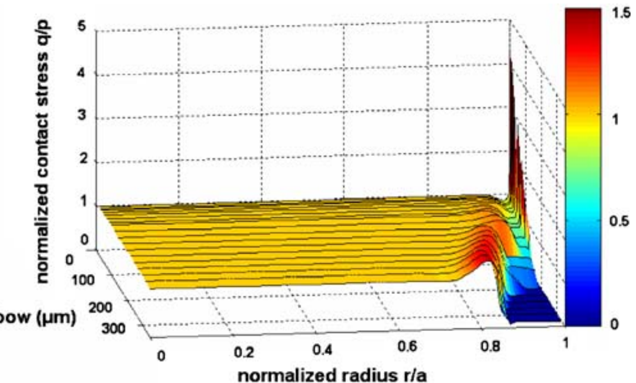

Fig. 13 A complete map to illustrate the relationship between contact stress, initial bow (convex type), and applied loading

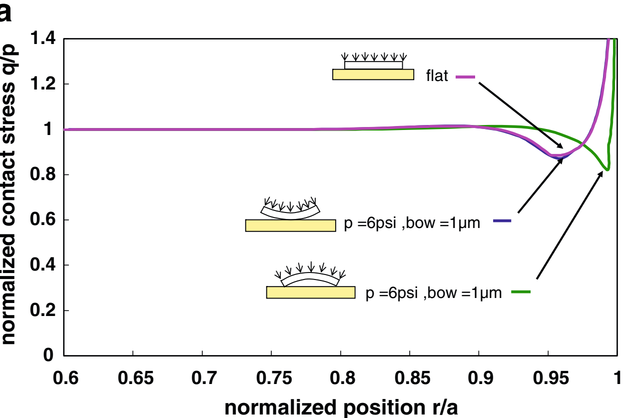

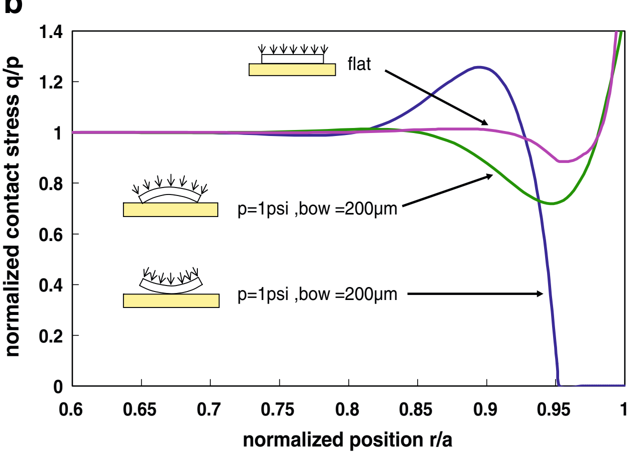

Fig. 14 Two typical contact stress distributions. **a** Low initial bow (±1 μm) with a high applied load (6 psi) and **b** high initial bow (±200 μm) with a low applied loading (1 psi)

concentric axisymmetric loads. Such a multiple-zone loading manner allows the users to adjust the magnitude (and perhaps the geometric parameters) of the loads to enhance the uniformity of the normal contact stress. In this subsection, for demonstration of the possible advantage of using multizone loading, a two-zone model is selected (model E; schematic in Fig. 15), to explore the possibility of using two distinct loads to enhance the contact stress uniformity. With more loading zones added, the chance of yielding a better stress uniformity is further increased. Considering the practical perspective in CMP machines, it is less possible to change the geometric parameters of the CMP system. As a result, the geometric parameters are fixed and only the applied loadings are adjusted to examine the feasibility.

As shown in Fig. 16a, the loading at zone I is fixed as 10 KPa; by varying the loading at zone II, the normal contact stress distribution is discussed. The normal contact stress at zone II is strongly related to the applied load at zone II and it is possible to find a range in which the contact stress uniformity is better than that of a single uniform load. It is also possible to incorporate the wafer warping effect into the analysis. Figure 16b shows the two-zone loading on a wafer with an initial bow of 10 μm. In comparison with the situation shown in Fig. 12 for a uniform loading, the uniformity can be significantly improved. Although the analysis cannot produce an analytical relationship, it indicates that a multiple-zone loading is feasible in enhancing the contact stress uniformity. Further, it shows that the optimal solution for a more complicated situation can be achieved using finite-element analysis.

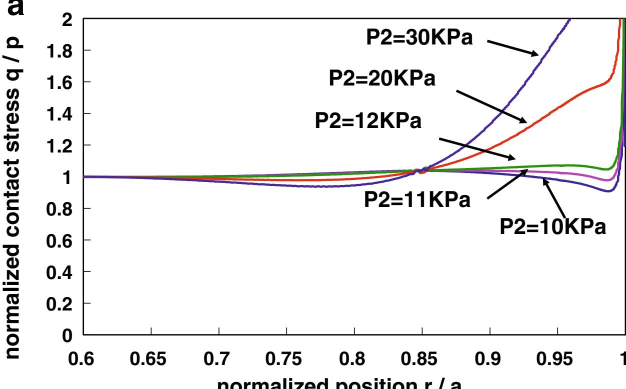

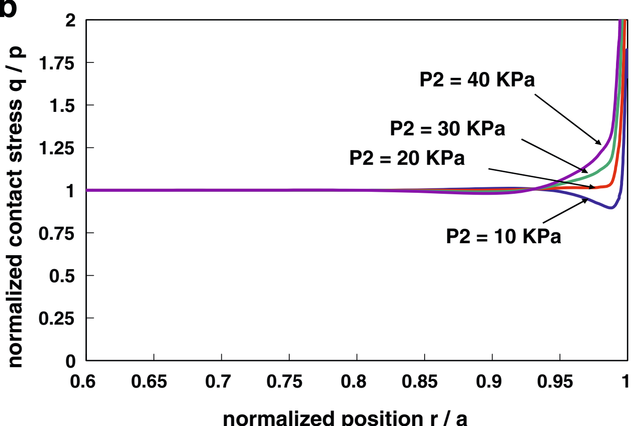

Fig. 16 **a** The contact stress distribution for a 10-KPa applied load at zone I with different applied loading at zone 2 and **b** the contact stress distribution for a 10-KPa applied load at zone I with different applied loading at zone II with an initial bow of 10 μm

5 Discussion

In this work, effects of major key parameters for CMP are revisited and results and conclusions differ from those of previous reports.

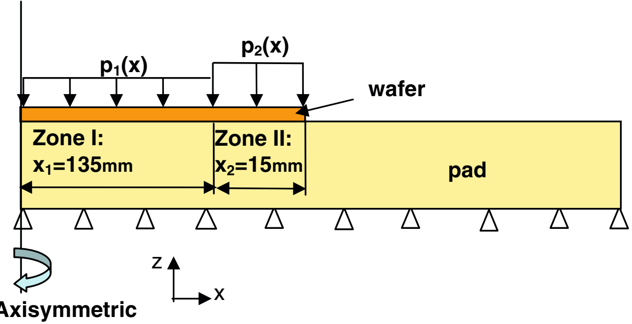

Fig 15 Schematic plot of a two-zone model

5.1 Revisited issues

- The traditional measure for CMP stress uniformity is improper and a new definition of CMP stress uniformity is proposed. The approach to enhance the CMP MRR uniformity is not to reduce the difference in contact stress between the wafer center and the edge but to extend the range of the normalized flat zone. Based on the range of normalized flat zone, the new definition for contact stress uniformity is more consistent and appears to be an appropriate performance index.
- Based on the new definition, unlike the previously reported conclusion, the stress distribution on the wafer surface is less dependent on the mechanical properties of the carrier film. This conclusion can be obtained even by applying simple concepts in elastic mechanics.
- The von Mises stress of the wafer or pad surface is dominated by the normal contact stress and both are essentially identical if the friction coefficient is small. However, with a higher friction coefficient, the difference between them may be large. Nevertheless, the

spatial distribution of these two stresses is similar. As a result, both stresses can be used as the local pressure (but with different Preston's constants).

- Theoretically, based on Fu and Chandra's work, the normal contact stress distribution is independent of the material properties of pads, and the simulation results agree with the prediction. However, the pad deformation is strongly related to the pad stiffness. As a consequence, the fluid pressure built would be different and the total effective normal contact stress would also be different for pads with different material properties.

5.2 New process parameters

- The effects of hyperelasticity from the polishing pad have been examined. The contact stress distributions are slightly different from those of linear elastic pads, especially under heavier loads. However, the difference is not significant. Rather, the major influence of material hyperelasticity is on the pad deformation and the possible contact pressure variation due to changes in slurry fluid pressure-which is deformation sensitive.
- The presence of the wafer bow due to thin-film residual stress may effectively reduce the normal contact stress uniformity. For situations with extremely high wafer bow, without sufficient loading, the wafer may not be in complete contact with the pad. This significantly affects the CMP efficiencies.
- Finite-element analysis of the contact between the wafer and the grooved pad indicates that the global normal

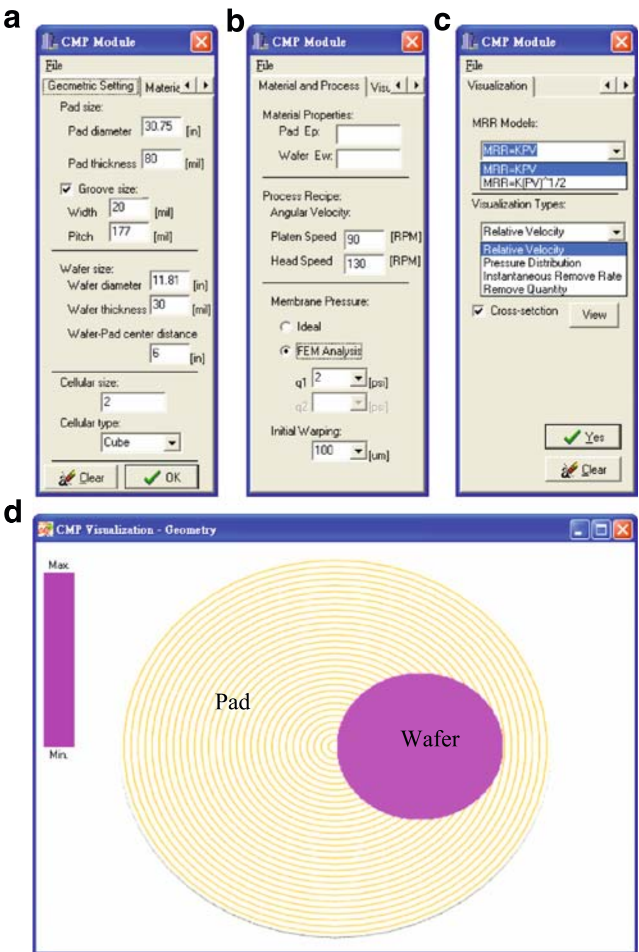

Fig. 17 The CMP CAD user interface, **a** geometric setting, **b** process recipe setting, **c** MRR models and visualization types, and **d** visualization window

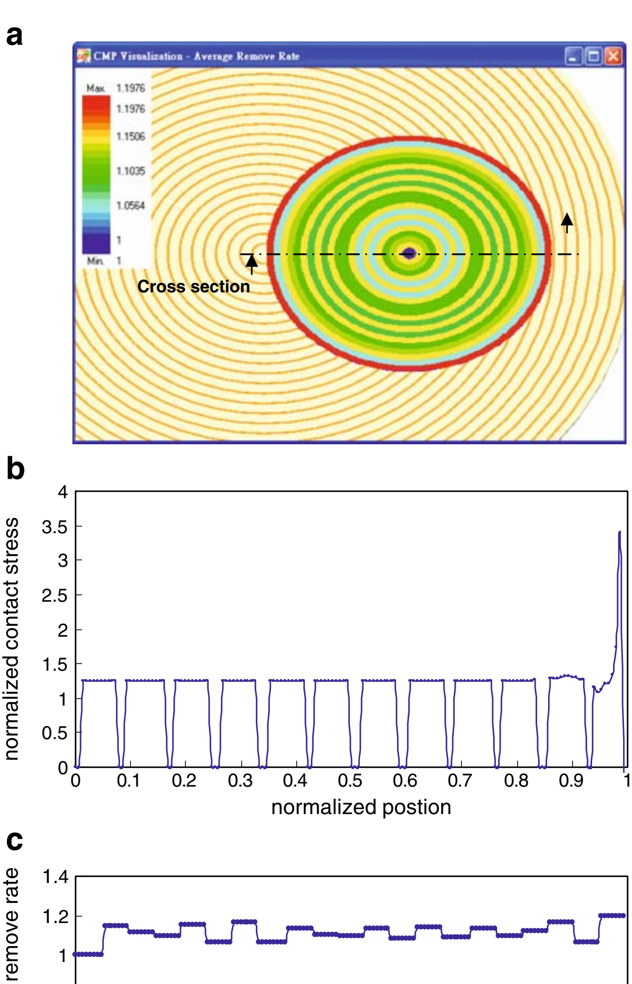

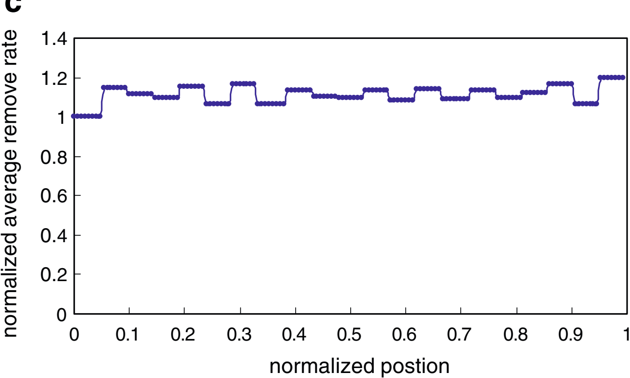

Fig. 18 The removing rate distribution of a grooved pad vs. bowed wafer (with a loading of 5 psi and a bow of 200 μm), **a** the removing rate contour, **b** normalized contact stress distribution, and **c** normalized average remove rate distribution for one revolution

contact stress distribution is essentially similar to that of the case of the flat wafer–pad contact multiplied by an effective contact area ratio.

- The finite-element simulation indicated that a multiple-zone load would be able to reduce the influence of the edge singularity and therefore increase the contact stress uniformity. The preliminary study shows that a two-zone loading may be sufficient. However, in order to count the fluid pressure variation built up under the wafer, the center portion might also require multiple loading setups. As a result, a three- to five-zone loading capability is recommended.

6 Applications: a CAD for wafer-level CMP analysis

A direct application of this work is to serve as the input and database for a CMP CAD currently developed by the authors. Based on a cellular automata approach [27] with the database provided, this CAD can provide clear information on contact stress contour, velocity distribution, material removal rate, and other parameters for various configurations. In addition, the solid mechanics provided in this study, together with research into fluid dynamics currently performed [28], should be able to offer a more detailed insight into the elastohydrodynamics perspective in CMP processes. Since the CAD application is not the main theme for this work, here, only a very brief introduction is provided to highlight the application of the above stress analyses. This wafer-level CMP CAD predicts the local material removal rate using Preston's equation or other models mentioned in "Section 2" [3–7]. These models correlate the MRR with relative velocities and stress distribution. The relative velocity between the wafer and the pad due to rotations and swings is modeled by kinematics. By the same token, Preston's constant is obtained experimentally. Finally, the stress distributions are obtained based on the above studies. Figure 17 shows a typical user interface of the CMP CAD. The averaged material removal rate contours, shown in Fig. 18, represent a contact example between a warped wafer and a grooved pad. The capability of the CAD can be further enhanced to cover the built-up fluid pressure, the material-property-dependent Preston's constant, and even chemical properties, to provide a more realistic prediction of the material removing rates.

7 Summary and conclusion

In this article, a detailed study of wafer-level contact stress distribution is performed using finite-element analyses for chemical–mechanical planarization applications. First, certain inconsistent issues observed from literature reviews, including the definition of CMP uniformity, the stress indicator, and the effect of carrier films, are investigated. For this category, a new definition of CMP uniformity based on the width of the relatively flat zone is proposed. In addition, the contact stress distribution in terms of both von Mises and normal stresses are investigated and their relationship is qualitatively established. Furthermore, the importance of the carrier films is reinvestigated and the conclusion indicates that their importance is not as significant as reported before. Based on the new definition, the effect of material parameters (linear elastic, hyperelastic), geometry parameters (carrier films, pad geometry, pad groove, wafer warping), and operating parameters (multi-zone applied loading) on the contact stress uniformity is analyzed and discussed. We found that the contact stress uniformity is degraded by the existence of wafer warping and a multiple-zone loading approach can improve the stress uniformity. These results should be useful in CMP process applications and subsequent CMP CAD development for improving the MRR uniformity.

Acknowledgement This work is supported by National Science Council of Taiwan under contract No. NSC-95-2221-E-006-037. The invaluable discussion and comments from Prof. T-S Yang and Mr. K-S Ou at NCKU are greatly appreciated.

References

1. Zantye PB, Kumar A, Sikder AK (2004) Chemical mechanical planarization for microelectronics applications. Mater Sci Eng Rep 45:89–220 doi:10.1016/j.mser.2004.06.002
2. Kim AT, Seok J, Tichy JA, Cale TS (2003) A multiscale elastohydrodynamic contact model for CMP. J Electrochem Soc 150:G570–G576 doi:10.1149/1.1598215
3. Preston F (1927) Optimization of computer controlled polishing. Glass Tech 11:214–219
4. Zhou C, Shan L, Hight JR, Ng SH, Danyluk S (2002) Fluid pressure and its effects on chemical mechanical polishing. Wear 253(3–4):430–437 doi:10.1016/S0043-1648(02)00155-2
5. Maury A, Ouma D, Boning D, Chung J (1997) A modification to Preston's equation and impact on pattern density effect modeling. Program Abstracts, Advanced Metalization and Interconnect Systems for ULSI Applications
6. Zhang F, Busnaina A (1998) The role of particle adhesion and surface deformation in chemical mechanical polishing processes. Electrochem Solid-State Lett 1(4):184–187 doi:10.1149/1.1390679
7. Zhao B, Shi FG (1999) Chemical mechanical polishing in IC processes: new fundamental insights. In: 1999 CMP-MIC conference, Santa Clara, CA, USA, pp 13–22
8. Runnels SR, Kim I, Schleuter J, Karlsrud C, Desai M (1998) A modeling tool for chemical–mechanical polishing design and evaluation. IEEE Trans Semicond Manuf 11:501–510 doi:10.1109/66.705385
9. Srinivasa-Murthy C, Wang D, Beaudoin SP, Bibby T, Holland K, Cale T (1997) Stress distribution in chemical–mechanical polish-

ing. Thin Solid Films 308:533–537 doi:10.1016/S0040-6090(97)00433-1
10. Wang D, Lee J, Holland K, Bibby T, Beaudoin S, Cale T (1997) Von Mises stress in chemical–mechanical polishing processes. J Electrochem Soc 144:1122–1127
11. Lin YY, Lo SP (2003) A study on the stress and nonuniformity of the wafer surface for the chemical–mechanical polishing process. Int J Adv Manuf Technol 22:401–409 doi:10.1007/s00170-003-1544-y
12. Lin YY, Lo SP (2004) A study of a finite element model for the chemical mechanical polishing process. Int J Adv Manuf Technol 23:644–650 doi:10.1007/s00170-002-1469-x
13. Lo SP, Lin YY (2005) The prediction of wafer surface non-uniformity using FEM and ANFIS in the chemical mechanical polishing process. J Mater Process Technol 168:250–257 doi:10.1016/j.jmatprotec.2005.01.010
14. Chiu JT, Lin YY (2008) Modal analysis of multi-layer structure for chemical mechanical polishing process. Int J Adv Manuf Technol 37:83–91 doi:10.1007/s00170-007-0960-9
15. Lo SP, Lin YY, Huang JC (2007) Analysis of retaining ring using finite element simulation in chemical mechanical polishing process. Int J Adv Manuf Technol 34:547–555 doi:10.1007/s00170-006-0622-3
16. Fu G, Chandra A (2005) The relationship between wafer surface pressure and wafer backside loading in chemical mechanical polishing. Thin Solid Films 474:217–221 doi:10.1016/j.tsf.2004.09.010
17. Tseng WT, Wang YH, Chin JH (1999) Effects of film stress on the chemical mechanical polishing process. J Electrochem Soc 146:4273–4280 doi:10.1149/1.1392627
18. Shiu SJ, Yu CC (2004) Multivariable control of multizone chemical mechanical polishing. J Vac Sci Technol B 22 (4):1679–1687 doi:10.1116/1.1761483
19. Liao YM, Yan HY, Wang FJ, Chen KS (2006) Mechanical properties characterization for CMP pads. In: 23rd National Conference of the Chinese Society of Mechanical Engineers, Tainan, Taiwan
20. Hibbit D, Karlsson B, Sorensen P (1998) ABAQUS/standard 5.8 user's manual. Hibbit, Karlsson, and Sorensen, Pawtucket
21. Johhnson KL (1985) Contact mechanics. Cambridge University Press, Cambridge
22. Runnels SR, Renteln P (1993) Modeling the effect of polish pad deformation on wafer surface stress distributions during chemical-mechanical polishing. Dielect Sci Technol 6:110–121
23. Baker AR (1997) The origin of the edge effects in CMP. Proc Electrochem Soc 96:228–237
24. Cook RD, Young WC (1999) Advanced mechanics of materials. Prentice-Hall, Upper Saddle River
25. Ling FF, Lai WM, Lucca DA (2002) Fundamentals of surface mechanics: with applications. Springer, New York
26. Stoney GG (1909) The tension of thin metallic film deposited by electrolysis. Proc R Soc Lond, A Contain Pap Math Phys Character 82(553):172–175 doi:10.1098/rspa.1909.0021
27. Hubbard TJ, Antonsson EK (1997) Cellular automata in MEMS design. In Sens Mater Conf, Tokyo, Japan vol. 7, pp 437–448
28. Wang YC, Yang TS (2007) Effects of pad grooves on chemical mechanical planarization. J Electrochem Soc 154(6):H486–H494 doi:10.1149/1.2716558